

Depinning free of the elastic approximation

A. B. Kolton ^{1,2}, E. E. Ferrero ^{3,4} and A. Rosso ⁵

¹Centro Atómico Bariloche, CNEA, CONICET, Bariloche R8402AGP, Argentina

²Instituto Balseiro, Universidad Nacional de Cuyo, Bariloche R8402AGP, Argentina

³Instituto de Nanociencia y Nanotecnología, CNEA–CONICET, Centro Atómico Bariloche, R8402AGP S. C. de Bariloche, Río Negro, Argentina

⁴Departament de Física de la Matèria Condensada & UBICS, Universitat de Barcelona, Martí i Franquès 1, 08028 Barcelona, Spain

⁵Université Paris-Saclay, LPTMS, CNRS, 91405 Orsay, France



(Received 23 June 2023; revised 19 September 2023; accepted 3 October 2023; published 1 November 2023)

We model the isotropic depinning transition of a domain wall using a two-dimensional Ginzburg-Landau scalar field instead of a directed elastic string in a random media. An exact algorithm accurately targets both the critical depinning field and the critical configuration for each sample. For random bond disorder of weak strength Δ , the critical field scales as $\Delta^{4/3}$ in agreement with the predictions for the quenched Edwards-Wilkinson elastic model. However, critical configurations display overhangs beyond a characteristic length $l_0 \sim \Delta^{-\alpha}$, with $\alpha \approx 2.2$, indicating a finite-size crossover. At large scales, overhangs recover the orientational symmetry which is broken by directed elastic interfaces. We obtain quenched Edwards-Wilkinson exponents below l_0 and invasion percolation depinning exponents above l_0 . A full picture of domain-wall isotropic depinning in two dimensions is hence proposed.

DOI: [10.1103/PhysRevB.108.174201](https://doi.org/10.1103/PhysRevB.108.174201)

I. INTRODUCTION

In recent decades, significant progress has been made in understanding a paradigmatic example of out-of-equilibrium critical phenomena: the depinning transition of elastic interfaces in random media [1–4]. Depinning is relevant in various extended physical systems, such as ferromagnetic [5] and ferroelectric [6,7] driven domain walls (DWs), tensioned cracks in hard and soft matter [8–10], the displacement of contact lines of liquid menisci [11–13], or even stressed tectonic plates and earthquakes [14,15]. The common basic phenomenology of the depinning transition is well captured by the simple model of a driven overdamped elastic interface coupled to a quenched disordered energy landscape that tends to trap the interface in configurations in which the potential energy is locally minimized. Under the application of a uniform external driving force f , the energy potential tilts. The interface might move slightly, but if the amplitude of the driving force is below a well-defined threshold f_c , it eventually pins and remains immobile. Instead, it sets into a steady-state motion, with an average velocity $v > 0$, if the driving force is above f_c . Exactly at f_c , the interface accommodates in a critical depinning configuration, exhibiting interesting universal geometrical properties.

Most progress in the field has been made by approximating the interface as *univalued* and using smooth scalar displacement fields for its dynamics, modeling it with overdamped equations like the driven quenched-Edwards-Wilkinson (qEW) model. Through powerful analytical and numerical techniques, researchers have found that the depinning transition at f_c is continuous, nonhysteretic, and occurs at a well-defined characteristic threshold force f_c [16]. At f_c , the interface is marginally blocked and the instability is described by a localized soft spot or eigenvector [17]. Just above the

threshold, the mean velocity v follows the depinning law $v \sim (f - f_c)^\beta$, with β being a nontrivial critical exponent [18]. A divergent correlation length $l \sim (f - f_c)^{-\nu}$ and a divergent correlation time $\tau \sim l^z$ characterize the jerky motion as f_c is approached from above. Below the length scale l , the rough geometry of the interface becomes self-affine (SA), with the displacement field growing as $u \sim x^\zeta$ for length scales x below l . Hence, $v \sim l^{\zeta-z}$ and $\beta = \nu(z - \zeta)$. Depinning critical exponents have been studied both analytically [19,20] and numerically [21–27]. Different universality classes are determined by the dimension of the interface d , the range [28–32] or nature [33] of the elastic interactions, the anisotropic [34] or isotropic correlations of the pinning forces [35,36], and the presence of additional nonlinear terms [34,37–41]. If the so-called statistical tilt symmetry holds, only two exponents are needed to fully characterize the depinning universality class. At large velocities, the effect of disorder mimics thermal fluctuations, and $v \sim f$. For $f < f_c$, motion is only possible through thermal activation at a finite temperature T . Particularly, for $f \ll f_c$ and relatively small temperatures, the universal creep-law [42–44] $\ln v(f) \sim -f^{-\mu}/T$ holds, with μ being a critical exponent related to dimension and the roughness exponent of the SA interface at thermal equilibrium ($f = 0$). Remarkably, in this ultraslow creep regime, a depinning criticality emerges at large scales, as observed both in the steady-state geometry and spatiotemporal fluctuations [45–49]. Furthermore, several of these qEW predictions are quantitatively confirmed by experiments conducted on ultrathin ferromagnetic films with perpendicular anisotropy [5,49–53].

However, the success of the elastic theory conflicts with the observation that, in the same experimental systems, DW configurations often exhibit *overhangs and pinch-off loops*,

which, in fact, challenge the assumptions of the elastic theory. The natural question that arises is *Why, then, does the theoretically minimalist approach of a purely elastic interface work so well?*

It is a common experimental practice to focus the analysis in a region displaying a well-behaved univalued DW segment far from the nucleation centers and rare defects to test the theory. However, it is not clear whether overhangs are generated solely by rare strong pinning centers or extrinsic defects, as suggested by Ferré *et al.* [5], or whether they are generated by intrinsic defects that act cooperatively. This type of intrinsic disorder is characterized by statistically uniform weak disorder with short-range correlations, as assumed in the elastic theory. In other words, overhangs, fingers, and bubbles might be part of the solution of the actual critical interface in weak disorder and not an issue to be avoided. Understanding why and to what extent the elastic theory applies is an important open question to gain a full understanding of the DW dynamics.

In this paper, using a disordered scalar Ginzburg-Landau (GL) model [54–57], which does not break isotropy, we free ourselves from the elastic approximation, allowing for plasticity and realistic deformations of the interface. With the help of an accurate algorithm, the critical fields and interface configurations can be solved at depinning for different realizations of the disorder. Our analysis ultimately provides a comprehensive picture of DW depinning in two-dimensional isotropic media with short-range correlated disorder. Critical configurations always display overhangs beyond a characteristic length l_0 that depends on the disorder strength Δ , indicating a finite-size crossover. Below l_0 , we obtain quenched Edwards-Wilkinson exponents, and above l_0 we observe invasion percolation depinning exponents.

It's worth mentioning that other approaches to the isotropic depinning transition have been pursued. Numerical simulations of the random-field Ising model (RFIM) suggest that, in two dimensions, the DW critical configurations at the depinning threshold should be either faceted or self-similar (SS), instead of the SA geometry predicted by the elastic theory [58,59]. However, these simulations are unable to address the isotropic depinning transition in the relevant weak disorder case due to the coupling of their thin DWs to the underlying periodic lattice [59], which breaks isotropy.

The paper is organized as follows: Section II introduces the model. Section III presents the algorithm that we developed to target the critical configurations at depinning. In Sec. IV, we describe and discuss our numerical results: First, the critical field (Sec. IV A) and then the geometry of the critical configurations (Sec. IV B). In Sec. IV B 3, we summarize our conclusions. The Appendix contains further details of the numerical computations.

II. MODEL

We consider the following time-dependent GL equation for a scalar order parameter field $\phi(x, y)$, describing approximately the zero-temperature evolution of the out-of-plane magnetization in a ferromagnetic film with perpendicular anisotropy [54–57]:

$$\gamma \partial_t \phi = c \nabla^2 \phi + \epsilon_0 [(1 + r(x, y))\phi - \phi^3] + h. \quad (1)$$

Here, the elastic constant c , ϵ_0 , and the friction γ are positive constants, h is the constant and uniform magnetic field, and $r(x, y)$ is a quenched random bond disorder specified by

$$\begin{aligned} \overline{r(x, y)} &= 0, \\ \overline{r(x', y')r(x, y)} &= \frac{2}{3} \Delta^2 \delta(x - x') \delta(y - y'). \end{aligned} \quad (2)$$

We denoted $\overline{(\dots)}$ the average over disorder realizations and Δ the disorder strength. We are interested in the limit of small disorder where the ground state at zero field is ferromagnetic (i.e., either $\phi \approx 1$ or $\phi \approx -1$).

We prepare the system with a small positive domain, namely, $\phi \approx 1$ for $y < y_0$ and $\phi = -1$ for $y > y_0$. After an initial transient at $h = 0$, we observe a well-defined DW of width $\delta \approx \sqrt{c/\epsilon_0}$ and surface tension (DW energy per unit length) $\sigma \approx \sqrt{c\epsilon_0}$. The location of the wall is defined as the level zero set of the magnetization, i.e., the set of points (x^*, y^*) , where $\phi(x^*, y^*) = 0$. Upon the application of a magnetic field h (that favors the positive ϕ phase) the domain wall would acquire a steady velocity $v(h) = mh$, with $m \approx \delta/\gamma$ the mobility of the wall; but in the presence of disorder, the velocity-field characteristics become nonlinear and display a depinning transition: above a threshold field h_a , the DW slides at a finite velocity, while below it the wall gets trapped into one of many metastable states. This has been clearly observed and quantified even in these scalar GL models where interfaces are not forced to be univalued [54]. Our goal is to determine h_a , and the last metastable state or critical configuration $\phi_d(x, y)$, as $h \rightarrow h_a$ from below.

III. ALGORITHM

Equation (1) is discretized with a regular $L \times L$ grid with coordinates (i, j) :

$$\begin{aligned} \partial_t \phi_{i,j} &= c[\phi_{i+1,j} + \phi_{i-1,j} + \phi_{i,j+1} + \phi_{i,j-1} - 4\phi_{i,j}] \\ &+ \epsilon_0[(1 + r_{i,j})\phi_{i,j} - \phi_{i,j}^3] + h = 0. \end{aligned} \quad (3)$$

Here, $r_{i,j}$ are uncorrelated random numbers sampled from a uniform distribution in $[-\Delta, \Delta]$. Setting $0 < \Delta < 1$, the term proportional to ϵ_0 in Eq. (3) always admits three zeros for $|\phi_{i,j}| < 1$. We apply periodic boundary conditions in the x direction $\phi_{i+L,j} = \phi_{i,j}$, but antiperiodic boundary conditions in the y direction, $\phi_{i,L} = -\phi_{i,0}$, to ensure that the evolution affects a single domain wall.

Starting from an arbitrary initial configuration (typically with a flat interface), we evolve the scalar field $\phi_{i,j}$ according to the so-called variant Monte Carlo method [24,38,60]. An elementary move updates $\phi_{i,j}$ by replacing it to one of the roots of Eq. (3) with $\partial_t \phi_{i,j} = 0$. Using the François Viète formula for the cubic equation, we find at most three real roots. The root that we select is the closer to the initial position $\phi_{i,j}$. The elementary steps are repeated consistently over the sites (i, j) , until the (positive) mean velocity of the order parameter is smaller than a small cutoff $\epsilon = 10^{-4}$, signaling the proximity to a metastable state.

This strategy relies on the Middleton theorems. The no-passing theorem assures that the algorithm connects an arbitrary initial state with the critical configuration, whereas the forward-moving theorem justifies the approach of making only forward directed elementary moves [60]. This allows us

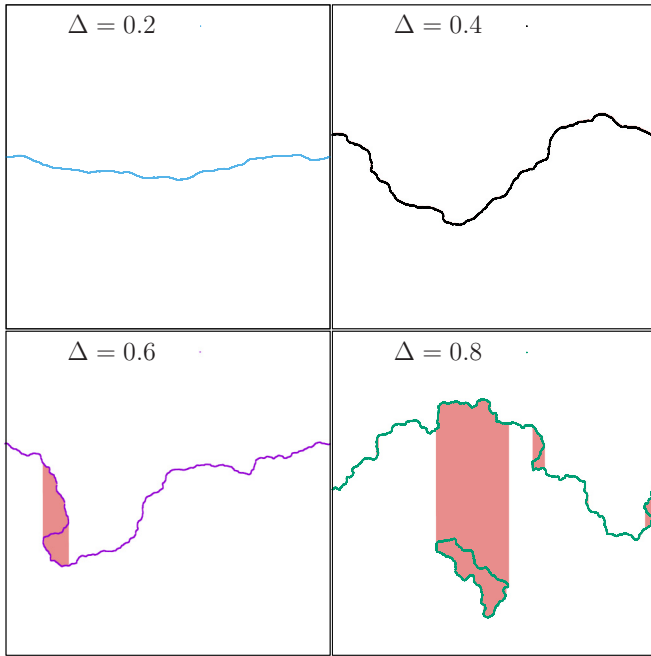


FIG. 1. Typical critical configurations of the domain wall for different values of the disorder strength Δ . System size is $L = 4096$ (the aspect ratio is one). Red shaded regions highlight overhangs and/or pinch-off loops.

to use the same technique developed in Refs. [24,38,60] for the elastic interface. The uniqueness of our implementation is that instead of applying it to the 1D DW displacement field, we apply it directly to the 2D order-parameter $\phi_{i,j}$. The order parameter is always univalued and bounded and has a convex elastic energy, though it can nucleate the multivalued critical DW we are more generally interested in. The algorithm proposed is, for a given accuracy, faster than the actual dynamics of Eq. (1) because elementary moves are not proportional to any numerical integration time step but instead controlled by a root finding method [61]. We thus alleviate the critical slowing down near all metastable states.

Furthermore, many of the computations involved in the implementation of the algorithm can be performed simultaneously, thus offering a valuable opportunity for an optimization via parallelization. These computations, such as elementary moves using the checkerboard decomposition, DW detection, and other image processing like routines and reductions to obtain properties are accelerated using graphics processors. To apply the algorithm, we discretize the two-dimensional space and use finite differences to evaluate the derivatives. We consider square systems of size $L \times L$. Without loss of generality, we choose $\epsilon_0 = 1$, $c = 1$, $\gamma = 1$, and for each disorder realization we draw $L \times L$ uncorrelated numbers $r(x, y)$ from a uniform distribution. The correlation length of the disorder r_f is thus of the order of the discretization itself and smaller than the DW width which then becomes the correlation length of the pinning force on DWs.

We build a sequence of metastable states as a function of h until we localize h_a , above which no metastable state can be found in the sample. Typical critical configurations for different values of Δ are shown in Fig. 1. Overhangs

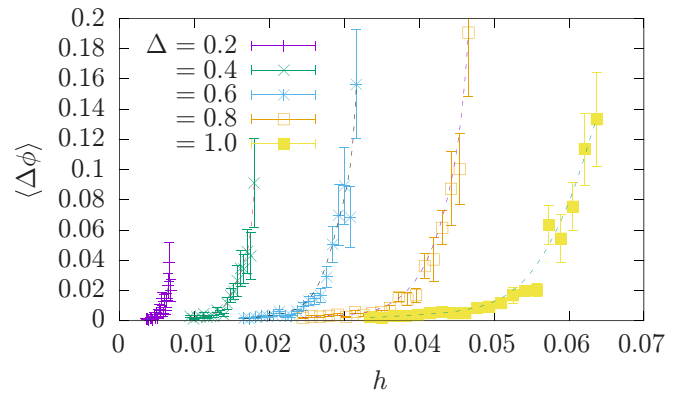


FIG. 2. Magnetization jump per site $\langle\phi\rangle$ as a function of h , for different values of the disorder strength Δ . Data correspond to averages over 50 samples, $L = 256$. Dashed-lines are guides to the eye.

can be clearly identified in the shaded areas (defined as the regions where the interface adopts more than one value in the advancement direction) and they are more frequent for large disorder. Interestingly, for the largest disorder we can also see isolated pinned pinch-off loops signaling domains that were not flipped.

The process of searching the root can be accelerated by a bisection method in the variable h . The critical field h_a can be thus obtained with the desired precision but with a price: the closer h_a , the larger the average simulation time due to the occurrence of large avalanches [62]. To illustrate this, we computed the magnetization jumps,

$$\langle\Delta\phi\rangle := \frac{1}{L^2} \sum_{i,j} [\tilde{\phi}_{i,j}(h + \delta h) - \tilde{\phi}_{i,j}(h)], \quad (4)$$

where $\tilde{\phi}_{i,j}(h)$ refers to the metastable configuration obtained at a given $h < h_a$.

In Fig. 2, the divergences for different values of $\Delta\phi$ are signatures of the h_a . The increase of h_a with increasing Δ can be appreciated. Notice that one could divide Eq. (4) by δh and interpret it as a generalized susceptibility $\chi \equiv \frac{\Delta\phi}{\delta h}$. Yet, its quantitative comparison with a true susceptibility in experiments would be meaningless at this point.

IV. RESULTS

Depending on the system size $L = 128, 256, \dots, 8192$, we obtain from hundreds to thousands of critical configurations of the DW, each one with their respective critical field h_a with an accuracy of $\Delta h_a = 10^{-4}$. This sampling allows us to perform statistics and analyze several properties. In Sec. IV A, we discuss the average over disorder of the critical field h_a for different values of the disorder Δ . In Sec. IV B, we discuss the geometry of the obtained critical configurations.

A. Critical field

We compute the average critical field h_a as a function of Δ for different sizes L . Figure 3 shows the power-law dependence $h_a \sim \Delta^{4/3}$. This result is consistent with Larkin's

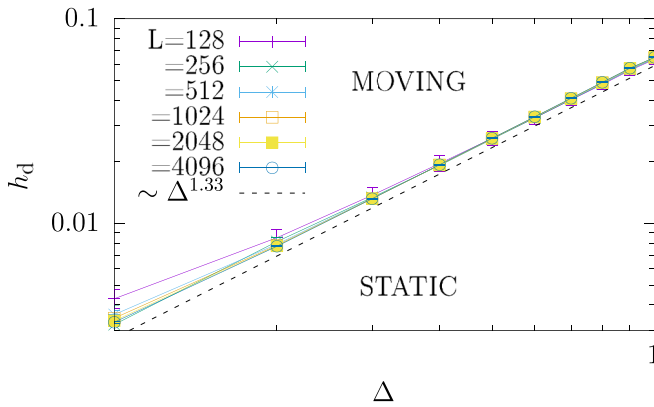


FIG. 3. Phase diagram of the domain-wall dynamics. A critical field h_d as a function of disorder strength Δ separates the static and moving phases. It displays a $h_d \sim \Delta^{1.33}$ in agreement with the predicted behavior $h_d \sim \Delta^{4/(4-d)}(\sigma\delta)^{-d/(4-d)}$ of weak collective pinning theory (dotted line). We display it for different system sizes L , finite-size effects are only observed for very small Δ .

prediction for weak collective pinning where $h_d \sim \sigma\delta l_c^{-2}$, with the Larkin length $l_c \approx (\sigma\delta/\Delta)^{2/(4-d)}$ (note that the microscopic pinning correlation length is the DW width δ). Finally, we have [63]

$$h_d \sim \Delta^{4/(4-d)}(\sigma\delta)^{-d/(4-d)}, \quad (5)$$

with $d = 1$ in our case. The deviations observed for small Δ and L can also be explained from the Larkin theory, since for small Δ , l_c becomes of the order of L . In this case, l_c is replaced by L , and thus $h_d \sim \sigma\delta L^{-2} > \sigma\delta l_c^{-2}$. The fact that the weak collective pinning theory is applicable shows that, at least up to the scale l_c , the DWs can successfully be described as a smooth elastic interface with univalued displacement field. It also shows that grid-pinning effects are negligible and that depinning is isotropic for the whole Δ range analyzed (see a detailed discussion in the Appendix).

We have also analyzed the sample-to-sample fluctuations of the depinning field h_d . These fluctuations are expected to scale with the size L of the interface as

$$\overline{[h_d - \bar{h}_d]^2} \sim L^{-2/\nu}, \quad (6)$$

For the 1D-qEW model of a SA interface, we expect $\nu \approx 4/3$. Quite surprisingly (or maybe not), the same exponent is expected for invasion percolation $\nu^{\text{IP}} \approx 4/3$. In Fig. 4, we plot the critical field fluctuations as a function of L for different values of Δ . The best fit (solid line) yields $[h_d - \bar{h}_d]^2 \sim \Delta^2 L^{-2/(1.27 \pm 0.1)}$, fairly close to $\nu \approx 4/3$ (dashed line) expected for the 1D-qEW model [26], the invasion percolation model [64], and also to the one observed in 2D-RFIM simulations with strong disorder [58]. In fact, we will argue that this is not just a coincidence.

B. Critical configurations

We now describe the geometrical properties of the configurations corresponding to the critical fields discussed in the previous section.

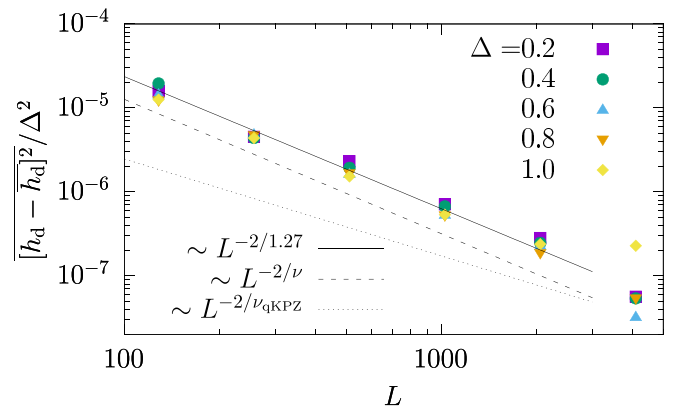


FIG. 4. Size dependence of the sample-to-sample fluctuations of the critical field for different disorder strengths Δ . Data is fairly described $\overline{[h_d - \bar{h}_d]^2} \sim \Delta^2 L^{1/1.27}$ (solid line), as can be appreciated by fitting the rescaled data. For comparison, we plot the scaling expected for the qEW model (dashed line) and for the qKPZ model (dotted line).

1. Overhangs

For a fixed L , depending on Δ , we find that there is a finite probability that the critical configuration presents overhangs (see insets of Fig. 5) and also pinch-off loops (see Fig. 1).

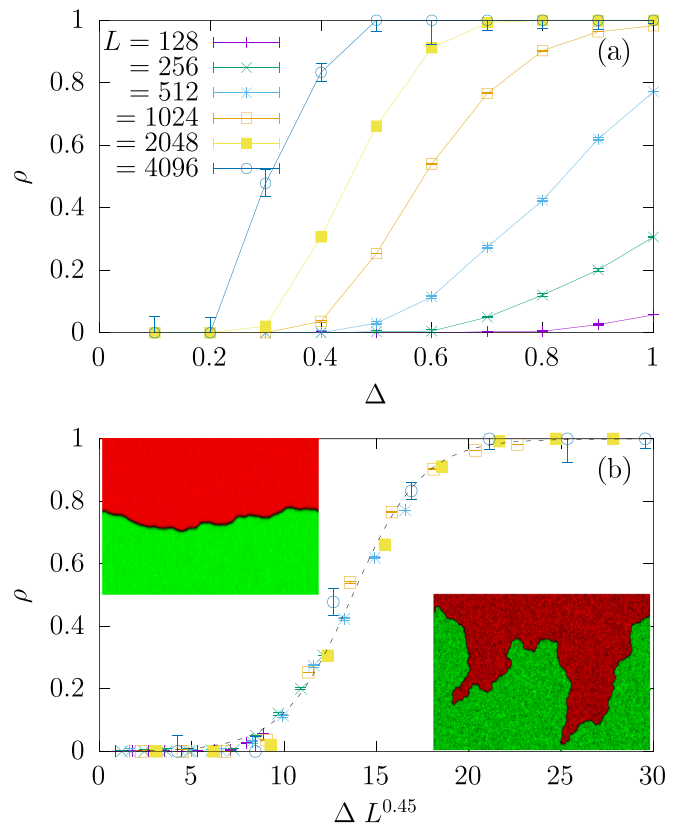


FIG. 5. Fraction ρ of multivalued domain walls at the depinning transition. (a) Raw data as a function of disorder strength Δ and transverse size L . (b) Scaled data, showing that $\rho(\Delta, L) \approx \tilde{\rho}(L/l_0)$ with $l_0 \sim \Delta^{-1/0.45}$. The inset shows typical domain walls for $L < l_0$ (left) and $L > l_0$ (right).

These are detected as multivalued DW displacements with respect to the reference flat initial configuration. We define the overhang probability ρ by counting, for a fixed L and Δ , the fraction of critical DW that presents overhangs for many randomness realizations. In Fig. 5(a), we see that always $\rho \rightarrow 1$ for large Δ , and $\rho \rightarrow 0$ for small Δ . Interestingly, the crossover depends on L , and the *empiric* scaling law $\rho(\Delta, L) \approx \tilde{\rho}(L/l_o)$, with

$$l_o \sim \Delta^{-1/0.45}, \quad (7)$$

decently fits the data for all the L and Δ values considered, as shown in Fig. 5(a). The success of this fit indicates that there exists a crossover length associated to the average overhang size, $l_o \sim \Delta^{-1/0.45}$. Since l_o diverges when $\Delta \rightarrow 0$ and not in a finite value of Δ , our results indicate that there is no transition to a phase of univalued interfaces but a disorder-driven crossover instead, and that DWs are always expected to present overhangs in the thermodynamic limit.

A simple heuristic argument can be used to relate the super-roughness predicted for the qEW model and the occurrence of overhangs. If we assume overhangs appear at the scale l where the extrinsic DW width or global roughness w satisfies $dw/dl \sim 1$ with $w \approx \delta(l/l_c)^\zeta$ and ζ the roughness exponent at that scale, we get

$$l_o \sim (l_c^\zeta/\delta)^{1/(\zeta-1)} \sim \Delta^{-\frac{2\zeta}{(4-d)(\zeta-1)}}. \quad (8)$$

Using that in $d = 1$ $l_c \sim \Delta^{-2/3}$, we need $\zeta \approx 1.43$ to obtain the observed exponent of $-1/0.45 \sim -2.2$ in the scaling of l_o with Δ . The value for this effective ζ remains to be explained, but lies in between the $d = 1$ Larkin exponent $\zeta_L = 3/2$ and the $d = 1$ depinning exponent $\zeta \approx 5/4$. More importantly, we note that, to obtain a finite $l_o > l_c$, the argument requires super-roughening ($\zeta > 1$) above l_c , and suggests that overhangs may not affect the SA geometry if $\zeta < 1$ (and for moderate Δ). This may explain why SA two-dimensional interfaces are observed in a three-dimensional space at depinning [65], using that $\zeta \approx 0.75$ for the 2D-qEW [24]. The argument then predicts one-dimensional SA critical interfaces in the long-range elasticity isotropic depinning case for which $\zeta \approx 0.39$ [30,31]. To test the scaling argument it would be interesting to address these predictions directly in future work.

2. Roughness exponent

In the previous sections, we have shown that DWs at the isotropic depinning transition always have overhangs in the thermodynamic limit. The existence of a large crossover length $l_o \sim \Delta^{-2.2} \gg l_c$ at weak disorder suggests that the random-manifold regime of the elastic theory may nevertheless exist at intermediate scales, where the probability of having one or more overhangs in a configuration is low. To test such a hypothesis, we next focus on the roughness of the critical configurations.

Standard methods to estimate the roughness exponent ζ of an interface rely on the existence of a univalued displacement field $u(x)$. We have shown, however, the interface at a given x can be multivalued, $\{u_n(x)\}_{n=1}^{m(x)}$, with $m(x) = 1, 3, 5, \dots$

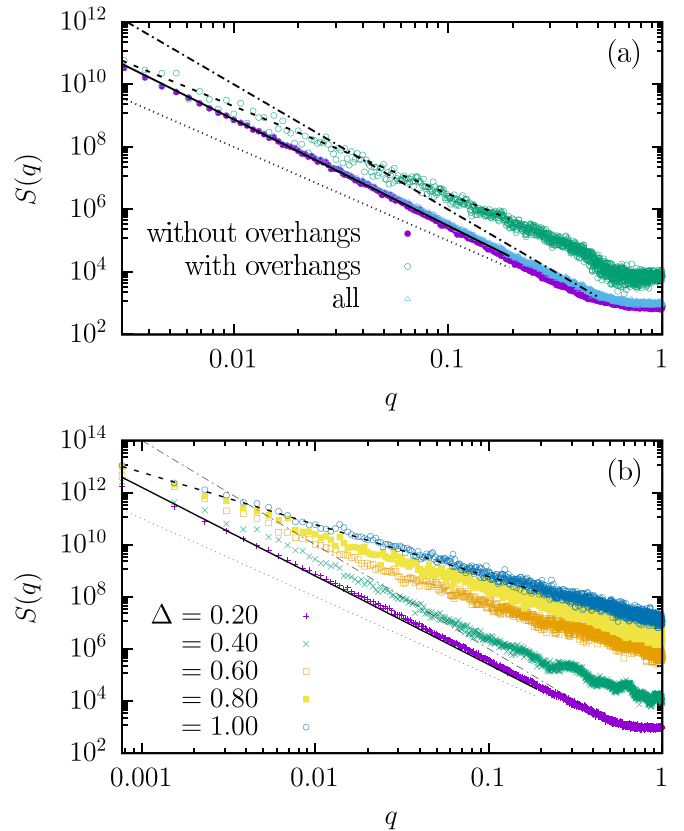


FIG. 6. Disorder-averaged structure factor $S(q)$ of domain-wall critical configurations. Data obtained for a system size $L = 8192$ (corresponding to a grid of $8192^2 \simeq 6.7 \times 10^7$ sites). (a) $S(q)$ averaged over configurations with overhangs, without overhangs, and averaged over all configurations (180 samples) for a fixed disorder strength $\Delta = 0.2$. Lines are guides to the eye and display pure power laws for $\zeta = 1.2$ (solid line) $\zeta = 1$ (dotted line), and $\zeta = 0.9$ (dashed line). (b) $S(q)$ averaged over all sampled critical configurations for increasing values of disorder strength Δ (180 samples for $\Delta = 0.2$, 50 samples for $\Delta > 0.2$). Guides-to-the-eye lines display pure power laws for $\zeta = 1.2$ (solid line) and $\zeta = 0.5$ (dashed line).

Hence, we define a univalued displacement field:

$$\tilde{u}(x) := \frac{1}{m(x)} \sum_{n=1}^{m(x)} u_n(x). \quad (9)$$

This particular choice coincides with the usual univalued interface if $m(x) = 1 \forall x$, but in the presence of overhangs it introduces artificial discontinuities in $\tilde{u}(x)$. Besides this warning, it is an operationally well-defined regularization, not only for simulation but also for experiments. A convenient way to obtain the roughness exponent at different length scales is through the structure factor

$$S(q) := \left| \sum_{x=1}^L e^{iqx} \tilde{u}(x) \right|^2 \sim \frac{1}{q^{1+2\zeta}}. \quad (10)$$

In Fig. 6(a), we show $S(q)$ for $\Delta = 0.2$ and $L = 8192$. For these parameters, $\rho \approx 0.2$, so—on average—one over five critical configurations is expected to have one or more overhangs. If we separate the contributions from interfaces

with and without overhangs, we can observe marked differences. For low q , in the case without overhangs, we can very accurately fit an exponent $\zeta \approx 1.2$ (solid line) which is compatible with the reported values $\zeta \approx 1.25$ for the 1D-qEW at depinning [5]. In the case with overhangs, we can reasonably fit (dashed line) an effective exponent $\zeta_{\text{eff}} = 0.9$ over the low- q region, even if overhangs have an important effect for the whole range of q . For the chosen value $\Delta = 0.2$, the average over all configurations (with and without overhangs) is dominated by the ones without overhangs. Nevertheless, as we increase Δ (or increase L) the configurations with overhangs dominate the average. In Fig. 6(b), we show the results for increasing values of Δ , the value of ζ_{eff} decreases with increasing Δ and tends to an exponent $\zeta_{\text{eff}} \approx 0.5$ [66].

The results of Fig. 6 support the applicability of the 1D-qEW model to describe DWs at depinning to scales below l_o , where overhangs are rare. On the other hand, overhangs produce lower effective roughness exponents. These must be interpreted carefully because they depend on our particular way to define \tilde{u} in Eq. (9). This result thus stresses the importance of a conscious interpretation of experimental data when $L > l_o$. More importantly, it stresses the importance of estimating quantitatively the crossover length l_o , both in experiments and simulations at the isotropic depinning transition.

3. Overhangs size scaling

In Fig. 6(b), we can see that for strong disorder $\zeta_{\text{eff}} \approx 0.5$, compatible with simple thermal roughening. One can interrogate whether this result is an artifact introduced by the regularization of Eq. (9) or rather an indication that a SA interface is emerging in spite of the presence of overhangs. To answer this question, with our model we analyze how the typical size of overhangs scales with the system linear size L . To do this, we first define

$$u_o^2 := \frac{1}{L} \sum_{x=1}^L \left[\sum_{n=1}^{m(x)} \frac{u_n(x)^2}{m(x)} - \left(\sum_{n=1}^{m(x)} \frac{u_n(x)}{m(x)} \right)^2 \right]. \quad (11)$$

The quantity between brackets [...] is identically zero if there is no overhang at x [since, in that case, $m(x) = 1$], and it is of the order of the overhang size squared otherwise (i.e., the variance of the multiple values of $u(x)$). Therefore, u_o gives the typical size of the overhangs in a given configuration (note that for a univalued function $u_o = 0$ regardless of its roughness).

In Fig. 7, we show that for $\Delta = 1$, u_o scales approximately linearly with L . This demonstrates that overhangs are relevant in the thermodynamic limit and can not be eliminated by coarse-graining. The snapshot shown on the right-side inset of Fig. 5 illustrates this result for a particular critical configuration. Therefore, the roughness exponent ζ_{eff} cannot be related to any emerging SA scale invariant. On the other hand, this suggests that overhangs allow us to recover the rotational symmetry, as they promote wandering of the local orientation of the DW. So, the final picture for the roughness of the DW is SA qEW \rightarrow finite size crossover \rightarrow SS (invasion percolation depinning), as larger length scales are tested.

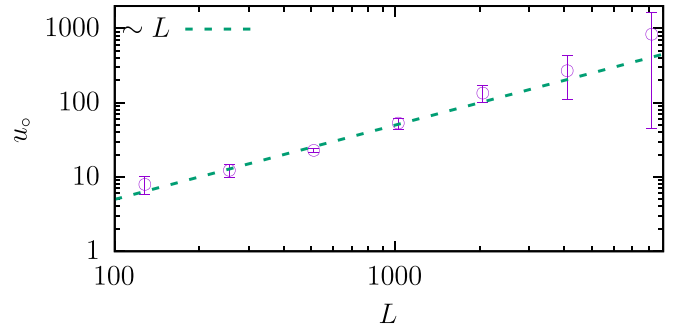


FIG. 7. Typical linear size of overhangs u_o [Eq. (11)] in the displacement direction as a function of the system size L for $\Delta = 1$. The dashed line is a guide to the eye with slope $\propto L$.

V. CONCLUSIONS

In summary, using an accurate algorithm, we showed that critical configurations at the isotropic depinning transition of one-dimensional DWs always present thermodynamically large overhangs in the thermodynamic limit. Rotational invariance is thus not broken at the isotropic depinning transition of $d = 1$ dimensional DWs in $d = 2$ random media. We find, nevertheless, a crossover length below which the predictions of the elastic theory of univalued interfaces predictions are well satisfied, including the qEW super-roughness. This extends the current theoretical understanding of depinning and reconciles it with many experimental observations where compatibility with the predictions for the 1D-qEW depinning universality class is found. We thus propose a full picture for the DW depinning in isotropic two dimensional media, which we hope will motivate further experimental and theoretical research on the depinning transition.

Our results could be relevant for experiments. While so far they can only compare at a qualitative level, the long-standing statistical physics questions addressed in our paper are important even for the experimental protocol conception and data analysis. For instance, work on magnetic DWs in the laboratory sometimes avoid including in the analysis nonunivalued pieces of interface and/or disregard pinch-offs as rare impurities related occurrences. We could now argue that those are not things to avoid, that they make part of the isotropic depinning theory and play a role in preserving the DW characteristics. We then hope that our paper could motivate a another look to experimental data (even the already existent one), perhaps not only in magnetic DWs but also on different experimental realizations of 1D DWs in 2D random media.

ACKNOWLEDGMENTS

We thank F. Paris for early discussions. We acknowledge support from the Centre National de la Recherche Scientifique (France) IRP Project Statistical Physics of Materials, and AGENCIA I+D+i PICT 2019 N° 1991 (MinCyT), and UNCuyo No. C014-T1 and CONICET Project PIP 2021 N° 0757. A.B.K. acknowledges hospitality at the LPTMS group where this project started. E.E.F. acknowledges support from the Maria Zambrano program of the Spanish Ministry of Universities through the University of Barcelona, and MCIN/AEI

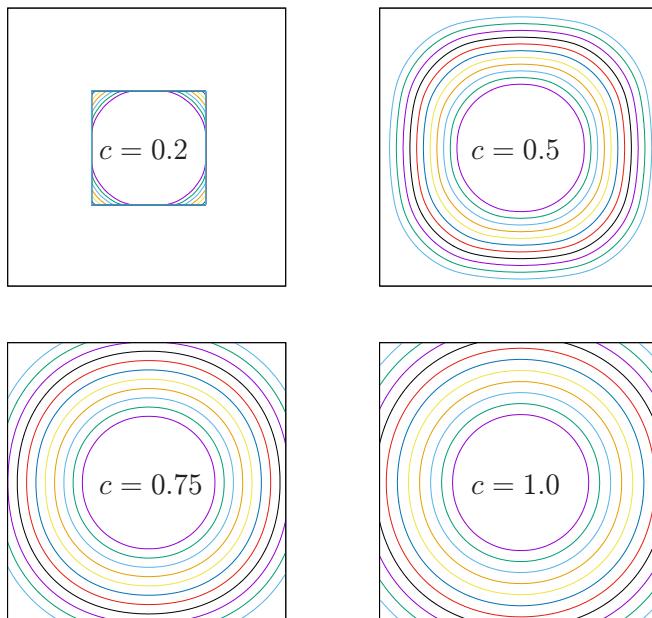


FIG. 8. Blowing an initially circular domain with a constant field $h = 0.1$ for $\epsilon_0 = 1$ and different values of c as indicated, corresponding to different values of the DW width $\delta \approx \sqrt{c/\epsilon_0}$. Lines of different colors corresponds to DW configurations at regularly distributed times.

support through No. PID2019-106290GB-C22. We have used computational resources from CCAD-UNC and GF-CNEA, which are part of SNCAD-MinCyT, Argentina.

APPENDIX: CONTROL OF LATTICE EFFECTS

To solve Eq. (1) numerically, a finite difference scheme based on an anisotropic regular lattice is typically used. If one wants to simulate isotropic depinning, it is important to assure that the effect of the discretization is negligible. This effect can be greatly reduced and put under control by choosing the DW width δ large enough. The smoother the interface, the weaker the effect of the mesh. Yet, a very wide DW requires larger systems to study the critical behavior. To choose a reasonable value of $\delta \approx \sqrt{c/\epsilon_0}$, we perform two numerical experiments.

First, we test the relevance of the anisotropic effect induced by the mesh by blowing an initially circular domain in the absence of disorder. We seed a circular domain at the center of the system and directly solve the dynamics of Eq. (1) at a constant field $h = 0.1$ for different DW widths by fixing $\epsilon_0 = 1$ and varying c . In Fig. 8, we observe that small values of c ($c = 0.2$ and $c = 0.5$) lead to an anisotropic growth that deviates from the circular shape. Further, one can see that the growth mean velocity is changing due to the mesh effect, since concentric lines correspond to regularly distributed times and they come closer to each other. For $c = 0.2$, the artificial periodic pinning is even able to pin the interface into

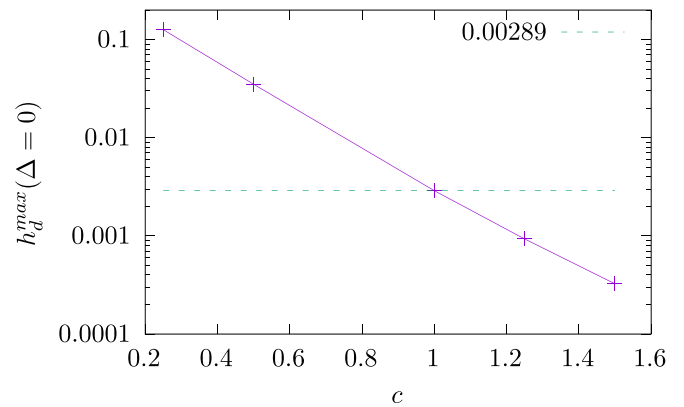


FIG. 9. Maximum depinning field h_d^{\max} in the absence of disorder ($\Delta = 0$) due to the effect of the square numerical mesh versus the order parameter elastic constant c . The dashed-line indicates h_d^{\max} for the parameters used to obtain our results in the main text.

a square metastable configuration. Fortunately, at larger values of c the undesired anisotropic effect rapidly vanishes ($c = 0.75$ displays circular configurations and for $c = 1$ we cannot detect any sign of anisotropy). Note that in the latter case, $\delta \approx 1$, a width comparable with the lattice spacing. The uncorrelated disorder increases system isotropy because rough DWs cannot coherently couple to the underlying periodic potential.

To go further, we also compute the pinning field h_d induced purely from the mesh in the absence of disorder ($\Delta = 0$) and compare it with the whole range of h_d values that we analyzed in Fig. 3 for different disorder strengths Δ . As for the case $c = 0.2$, $h = 0.1$, the maximum pinning field $h_d^{\max}(\Delta = 0)$ is associated to a square DW. In Fig. 9, we show $h_d^{\max}(\Delta = 0)$, computed using our exact algorithm, as a function of the elastic constant c . We can observe that it decreases approximately exponentially with increasing c , (i.e., increasing the DW width). In particular, for the choice $c = 1$ that we adopted to obtain most of the results in our paper, we get $h_d^{\max}(\Delta = 0) \approx 0.00289$, much smaller than the critical field obtained for the weakest disorder considered ($\Delta = 0.1$). Therefore, we conclude the mesh pinning does not affect our results. For even smaller Δ values, it may be necessary to increase the DW's intrinsic width $\delta \sim \sqrt{c/\epsilon_0}$, either increasing c or decreasing ϵ_0 . Figure 9 can be used as a general guide for that.

In summary, we find that anisotropic effects can be kept under control for any disorder strength. Our method thus constitutes an essential improvement over models of discrete scalar fields: In the 2D-RFIM DWs are *always* sharp. In particular, in the limit of weak disorder, square domains are not avoidable already at $\Delta \sim 1$ [58,59]. Figure 3 shows that these kind of effects are absent in our simulations. Therefore, our approach allows us to test the prediction of the elastic theory in isotropic depinning.

[1] M. Kardar, *Phys. Rep.* **301**, 85 (1998).

[2] T. Nattermann and S. Scheidl, *Adv. Phys.* **49**, 607 (2000).

[3] D. S. Fisher, *Phys. Rep.* **301**, 113 (1998).

[4] K. J. Wiese, *Rep. Prog. Phys.* **85**, 086502 (2022).

- [5] J. Ferré, P. J. Metaxas, A. Mougin, J.-P. Jamet, J. Gorchon, and V. Jeudy, *C. R. Phys.* **14**, 651 (2013), Disordered systems.
- [6] W. Kleemann, J. Rhensius, O. Petracic, J. Ferré, J. P. Jamet, and H. Bernas, *Phys. Rev. Lett.* **99**, 097203 (2007).
- [7] P. Paruch and J. Guyonnet, *C. R. Phys.* **14**, 667 (2013), Disordered systems.
- [8] D. Bonamy, S. Santucci, and L. Ponsou, *Phys. Rev. Lett.* **101**, 045501 (2008).
- [9] L. Ponsou, *Phys. Rev. Lett.* **103**, 055501 (2009).
- [10] C. Le Priol, J. Chopin, P. Le Doussal, L. Ponsou, and A. Rosso, *Phys. Rev. Lett.* **124**, 065501 (2020).
- [11] J. F. Joanny and P. G. de Gennes, *J. Chem. Phys.* **81**, 552 (1984).
- [12] S. Moulinet, A. Rosso, W. Krauth, and E. Rolley, *Phys. Rev. E* **69**, 035103(R) (2004).
- [13] P. L. Doussal, K. J. Wiese, S. Moulinet, and E. Rolley, *Europhys. Lett.* **87**, 56001 (2009).
- [14] E. A. Jagla and A. B. Kolton, *J. Geophys. Res.: Solid Earth* **115**, B5 (2010).
- [15] E. A. Jagla, F. P. Landes, and A. Rosso, *Phys. Rev. Lett.* **112**, 174301 (2014).
- [16] A. B. Kolton, S. Bustingorry, E. E. Ferrero, and A. Rosso, *J. Stat. Mech.: Theory Exp.* (2013) P12004.
- [17] X. Cao, S. Bouzat, A. B. Kolton, and A. Rosso, *Phys. Rev. E* **97**, 022118 (2018).
- [18] E. E. Ferrero, S. Bustingorry, A. B. Kolton, and A. Rosso, *C. R. Phys.* **14**, 641 (2013).
- [19] P. Le Doussal, K. J. Wiese, and P. Chauve, *Phys. Rev. B* **66**, 174201 (2002).
- [20] A. A. Fedorenko and S. Stepanow, *Phys. Rev. E* **67**, 057104 (2003).
- [21] H. Leschhorn, *Physica A* **195**, 324 (1993).
- [22] H. Leschhorn, T. Nattermann, S. Stepanow, and L.-H. Tang, *Ann. Phys.* **509**, 1 (1997).
- [23] L. Roters, A. Hucht, S. Lübeck, U. Nowak, and K. D. Usadel, *Phys. Rev. E* **60**, 5202 (1999).
- [24] A. Rosso, A. K. Hartmann, and W. Krauth, *Phys. Rev. E* **67**, 021602 (2003).
- [25] A. Rosso, P. Le Doussal, and K. J. Wiese, *Phys. Rev. B* **75**, 220201(R) (2007).
- [26] E. E. Ferrero, S. Bustingorry, and A. B. Kolton, *Phys. Rev. E* **87**, 032122 (2013).
- [27] E. E. Ferrero, S. Bustingorry, and A. B. Kolton, *Phys. Rev. E* **87**, 069901(E) (2013).
- [28] S. Ramanathan and D. S. Fisher, *Phys. Rev. B* **58**, 6026 (1998).
- [29] S. Zapperi, P. Cizeau, G. Durin, and H. E. Stanley, *Phys. Rev. B* **58**, 6353 (1998).
- [30] A. Rosso and W. Krauth, *Phys. Rev. E* **65**, 025101(R) (2002).
- [31] O. Duemmer and W. Krauth, *J. Stat. Mech.: Theory Exp.* (2007) P01019.
- [32] L. Laurson, X. Illa, S. Santucci, K. Tore Tallakstad, K. J. Måløy, and M. J. Alava, *Nat. Commun.* **4**, 2927 (2013).
- [33] H.-H. Boltz and J. Kierfeld, *Phys. Rev. E* **90**, 012101 (2014).
- [34] L.-H. Tang, M. Kardar, and D. Dhar, *Phys. Rev. Lett.* **74**, 920 (1995).
- [35] A. A. Fedorenko, P. Le Doussal, and K. J. Wiese, *Phys. Rev. E* **74**, 041110 (2006).
- [36] S. Bustingorry, A. B. Kolton, and T. Giamarchi, *Phys. Rev. B* **82**, 094202 (2010).
- [37] L. A. Nunes Amaral, A.-L. Barabási, and H. E. Stanley, *Phys. Rev. Lett.* **73**, 62 (1994).
- [38] A. Rosso and W. Krauth, *Phys. Rev. Lett.* **87**, 187002 (2001).
- [39] T. Goodman and S. Teitel, *Phys. Rev. E* **69**, 062105 (2004).
- [40] P. Le Doussal and K. J. Wiese, *Phys. Rev. E* **67**, 016121 (2003).
- [41] Y. J. Chen, S. Zapperi, and J. P. Sethna, *Phys. Rev. E* **92**, 022146 (2015).
- [42] L. B. Ioffe and V. M. Vinokur, *J. Phys. C* **20**, 6149 (1987).
- [43] T. Nattermann, *Phys. Rev. Lett.* **64**, 2454 (1990).
- [44] P. Chauve, T. Giamarchi, and P. Le Doussal, *Phys. Rev. B* **62**, 6241 (2000).
- [45] A. B. Kolton, A. Rosso, T. Giamarchi, and W. Krauth, *Phys. Rev. Lett.* **97**, 057001 (2006).
- [46] A. B. Kolton, A. Rosso, T. Giamarchi, and W. Krauth, *Phys. Rev. B* **79**, 184207 (2009).
- [47] E. E. Ferrero, L. Foini, T. Giamarchi, A. B. Kolton, and A. Rosso, *Phys. Rev. Lett.* **118**, 147208 (2017).
- [48] E. E. Ferrero, L. Foini, T. Giamarchi, A. B. Kolton, and A. Rosso, *Annu. Rev. Condens. Matter Phys.* **12**, 111 (2021).
- [49] M. P. Grassi, A. B. Kolton, V. Jeudy, A. Mougin, S. Bustingorry, and J. Curiale, *Phys. Rev. B* **98**, 224201 (2018).
- [50] S. Lemerle, J. Ferré, C. Chappert, V. Mathet, T. Giamarchi, and P. Le Doussal, *Phys. Rev. Lett.* **80**, 849 (1998).
- [51] V. Jeudy, R. Díaz Pardo, W. Savero Torres, S. Bustingorry, and A. B. Kolton, *Phys. Rev. B* **98**, 054406 (2018).
- [52] V. Jeudy, A. Mougin, S. Bustingorry, W. Savero Torres, J. Gorchon, A. B. Kolton, A. Lemaître, and J.-P. Jamet, *Phys. Rev. Lett.* **117**, 057201 (2016).
- [53] L. J. Albornoz, E. E. Ferrero, A. B. Kolton, V. Jeudy, S. Bustingorry, and J. Curiale, *Phys. Rev. B* **104**, L060404 (2021).
- [54] N. B. Caballero, E. E. Ferrero, A. B. Kolton, J. Curiale, V. Jeudy, and S. Bustingorry, *Phys. Rev. E* **97**, 062122 (2018).
- [55] N. Caballero, E. Agoritsas, V. Lecomte, and T. Giamarchi, *Phys. Rev. B* **102**, 104204 (2020).
- [56] P. C. Guruciaga, N. Caballero, V. Jeudy, J. Curiale, and S. Bustingorry, *J. Stat. Mech.: Theory Exp.* (2021) 033211.
- [57] N. Caballero, *J. Stat. Mech.: Theory Exp.* (2021) 103207.
- [58] H. Ji and M. O. Robbins, *Phys. Rev. A* **44**, 2538 (1991).
- [59] B. Koiller, H. Ji, and M. O. Robbins, *Phys. Rev. B* **46**, 5258 (1992).
- [60] A. Rosso and W. Krauth, *Comput. Phys. Commun.* **169**, 188 (2005).
- [61] The computational cost of the present algorithm is equivalent to the one applied to two-dimensional univalued interfaces (only the nonlinear force changes). We refer the reader to Ref. [24] for a discussion about its performance compared with the direct integration of the equation of motion of the 2D interface [i.e., the equivalent to Eq. (1)].
- [62] A. B. Kolton, A. Rosso, E. V. Albano, and T. Giamarchi, *Phys. Rev. B* **74**, 140201(R) (2006).
- [63] G. Blatter, M. V. Feigel'man, V. B. Geshkenbein, A. I. Larkin, and V. M. Vinokur, *Rev. Mod. Phys.* **66**, 1125 (1994).
- [64] S. Maslov, *Phys. Rev. Lett.* **74**, 562 (1995).
- [65] J. T. Clemmer and M. O. Robbins, *Phys. Rev. E* **100**, 042121 (2019).
- [66] It is worth noting that the decrease of ζ_{eff} with increasing Δ is similar to the behavior reported in Ref. [67] for the spectral roughness exponent in the 2D-RFIM using the Monte Carlo method.
- [67] X. P. Qin, B. Zheng, and N. J. Zhou, *J. Phys. A: Math. Theor.* **45**, 115001 (2012).